Crystal structure of repotrectinib, $C_{18}H_{18}FN_5O_2$

James A. Kaduk[1,2], Anja Dosen[3] and Tom Blanton[3]
[1]Department of Chemistry, Illinois Institute of Technology, 3101 South Dearborn Street, Chicago, IL 60616, USA
[2]Department of Physics, North Central College, 131 South Loomis Street, Naperville, IL 60540, USA
[3]International Centre for Diffraction Data (ICDD), 12 Campus Boulevard, Newtown Square, PA 19073-3273, USA

(Received 28 December 2024; revised 24 May 2025; accepted 30 May 2025)

Abstract: The crystal structure of repotrectinib has been solved and refined using synchrotron X-ray powder diffraction data and optimized using density functional theory techniques. Repotrectinib crystallizes in the space group $P2_12_12_1$ (#19) with a = 9.27406(5), b = 11.60810(8), c = 15.63623 (8) Å, V = 1,683.306(20) Å^3, and Z = 4 at 298 K. The crystal structure consists of stacks of V-shaped molecules along the b-axis. One amino group acts as a donor to the carbonyl group to link the molecules into chains along the a-axis with a graph set *C1,1(8)*. The second amino group forms two intramolecular hydrogen bonds. The powder pattern has been submitted to the International Centre for Diffraction Data for inclusion in the Powder Diffraction File™ (PDF®).

[doi:10.1017/S0885715625100882]

Key words: repotrectinib, Augtyro™, crystal structure, Rietveld refinement, density functional theory

I. INTRODUCTION

Repotrectinib (sold under the brand name Augtyro) is used for the treatment of cancer. Specifically, it is a tyrosine (https://pubchem.ncbi.nlm.nih.gov/compound/tyrosine) kinase inhibitor used for the treatment of locally advanced or metastatic ROS1-positive non-small cell lung cancer. The systematic name (CAS Registry No. 1802220-02-5) is (3R,11S)-6-fluoro-3,11-dimethyl-10-oxa-2,13,17,18,21-pentazatetracyclo[13.5.2.0^{4,9}.0^{18,22}] docosa-1(21),4(9),5,7,15(22),16,19-heptaen-14-one. A two-dimensional molecular diagram of repotrectinib is shown in Figure 1.

Repotrectinib is claimed in U.S. Patent 10294242 B2 (Cui and Rogers, 2019; TP Therapeutics), and powder diffraction data are provided. The crystal structures of repotrectinib complexed to two proteins have been reported (Murray et al., 2021; PDB entries 7VKN and 7VKO). Murray's paper indicates that the crystal structure of unbound repotrectinib was also determined, but we can find no evidence that the structure has been published or deposited.

This work was carried out as part of a project (Kaduk et al., 2014) to determine the crystal structures of large-volume commercial pharmaceuticals and include high-quality powder diffraction data for them in the Powder Diffraction File™ (Kabekkodu et al., 2024).

II. EXPERIMENTAL

Repotrectinib was a commercial reagent, purchased from TargetMol (Batch #T4071) and was used as received. The white powder was packed into a 0.5-mm-diameter Kapton capillary and rotated during the measurement at ~2 Hz. The powder pattern was measured at 298(1) K at the Wiggler Low Energy Beamline (Leontowich et al., 2021) of the Brockhouse X-ray Diffraction and Scattering Sector of the Canadian Light Source using a wavelength of 0.819563(2) Å (15.1 keV) from 1.6 to 75.0° 2θ with a step size of 0.0025° and a collection time of 3 minutes. The high-resolution powder diffraction data were collected using eight Dectris Mythen2 X series 1K linear strip detectors. NIST SRM 660b LaB_6 was used to calibrate the instrument and refine the monochromatic wavelength used in the experiment.

The pattern was indexed using N-TREOR as incorporated into EXPO2014 (Altomare et al., 2013) on a primitive orthorhombic unit cell with a = 9.27497(95), b = 11.60771(170), c = 15.63851(130) Å, V = 1,683.7 Å^3, and Z = 4. The suggested space group was $P2_12_12_1$, which was confirmed by the successful solution and refinement of the structure. A reduced cell search of the Cambridge Structural Database (Groom et al., 2016) yielded three hits, but no structures of repotrectinib or its derivatives.

The structure was solved by direct methods as incorporated into EXPO2014. Several atom types had to be reassigned manually. The positions of the hydrogen atoms were calculated using Mercury (Macrae et al., 2020). Mercury was also used to invert the structure to correspond more closely to that contained in PubChem (Kim et al., 2023).

Rietveld refinement was carried out with GSAS-II (Toby and Von Dreele, 2013). Only the 4.0–60.0° portion of the pattern was included in the refinements (d_{min} = 0.819 Å). All non-H-bond distances and angles were subjected to restraints, based on a Mercury/Mogul Geometry Check

Corresponding author: James A. Kaduk; Email: kaduk@polycrystallography.com

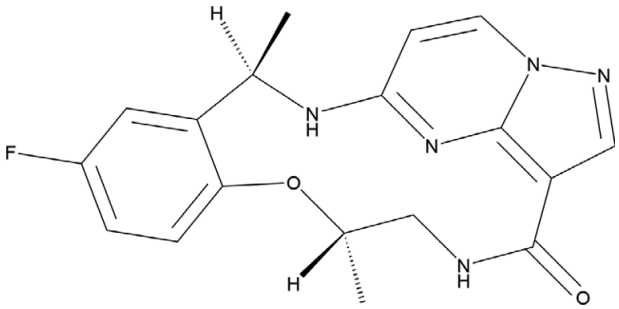

Figure 1. The two-dimensional structure of repotrectinib.

(Bruno et al., 2004; Sykes et al., 2011). The Mogul average and standard deviation for each quantity were used as the restraint parameters. The benzene and pyrazolo[1,5-*a*]pyrimidine ring systems were restrained to be planar. The restraints contributed 6.5% to the overall χ^2. The hydrogen atoms were included in calculated positions, which were recalculated during the refinement using Materials Studio (Dassault Systèmes, 2023). The U_{iso} of the heavy atoms were grouped by chemical similarity. The U_{iso} of the H atoms were fixed at 1.3× the U_{iso} of the heavy atoms to which they are attached. The peak profiles were described using the generalized (Stephens, 1999) microstrain model. The background was modeled using a six-term shifted Chebyshev polynomial, with peaks at 10.29 and 43.47° to model the narrow and broad scattering from the Kapton capillary and any amorphous component.

The final refinement of 102 variables using 22,401 observations and 73 restraints yielded the residual R_{wp} = 0.04561. The largest peak (1.39 Å from O2) and hole (1.20 Å from C22) in the difference Fourier map were 0.30(8) and − 0.30 (8) eÅ^{-3}, respectively. The final Rietveld plot is shown in Figure 2. The largest features in the normalized error plot are in the shapes of some of the strong low-angle peaks.

The crystal structure of repotrectinib was optimized (fixed experimental unit cell) with density functional theory techniques using VASP (Kresse and Furthmüller, 1996) through the MedeA graphical interface (Materials Design, 2024). The calculation was carried out on 32 cores of a 144-core (768-GB memory) HPE Superdome Flex 280 Linux server at North Central College. The calculation used the GGA-PBE functional, a plane wave cutoff energy of 400.0 eV, and a *k*-point spacing of 0.5 Å^{-1}, leading to a 2 × 2 × 1 mesh, and took ~7.3 hours. Single-point density functional calculations (fixed experimental cell) and population analysis were carried out using CRYSTAL23 (Erba et al., 2023). The basis sets for the H, C, and O atoms in the calculation were those of Gatti et al. (1994), and that for F was that of Peintinger et al. (2013). The calculations were run on a 3.5-GHz PC using eight *k*-points and the B3LYP functional and took ∼2.6 hours.

III. RESULTS AND DISCUSSION

This synchrotron powder pattern of repotrectinib matches the laboratory powder diffraction pattern reported by Cui and Rogers (2019) well enough to conclude that they represent the same material (Figure 3). The structures of the repotrectinib molecules in the two protein structures 7VKN and 7VKO are very similar; the root-mean-square (rms) Cartesian displacement is 0.118 Å. The molecular structures here and in 7VKN are essentially identical; the rms displacement is 0.162 Å.

The rms difference of the non-H atoms in the Rietveld-refined and VASP-optimized structures, calculated using the Mercury CSD-Materials/Search/Crystal Packing Similarity tool, is 0.078 Å. The rms Cartesian displacement of the non-H atoms in the Rietveld-refined and VASP-optimized structures of the molecule, calculated using the Mercury Calculate/Molecule Overlay tool, is 0.051 Å (Figure 4). The agreements are within the normal range for correct structures (van de

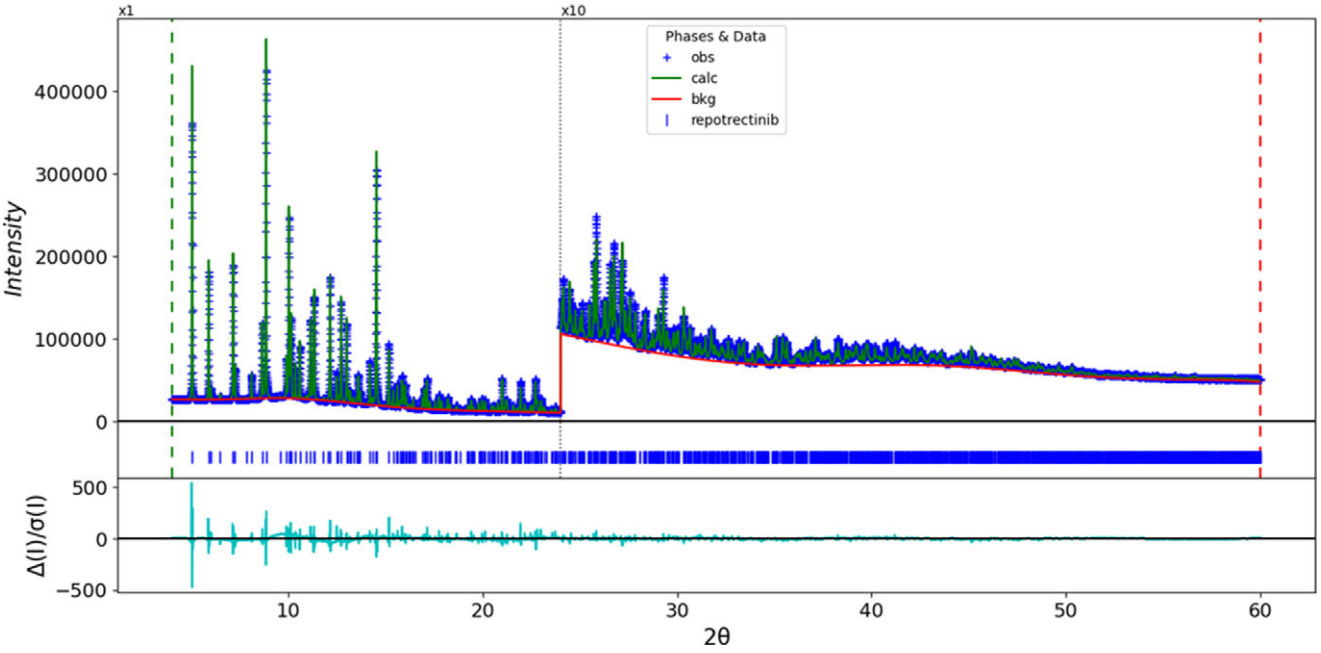

Figure 2. The Rietveld plot for repotrectinib. The blue crosses represent the observed data points, and the green line represents the calculated pattern. The cyan curve represents the normalized error plot, and the red line represents the background curve. The blue tick marks indicate the repotrectinib peak positions. The vertical scale has been multiplied by a factor of 10× for 2θ > 24.0°.

https://doi.org/10.1017/S0885715625100882 Published online by Cambridge University Press

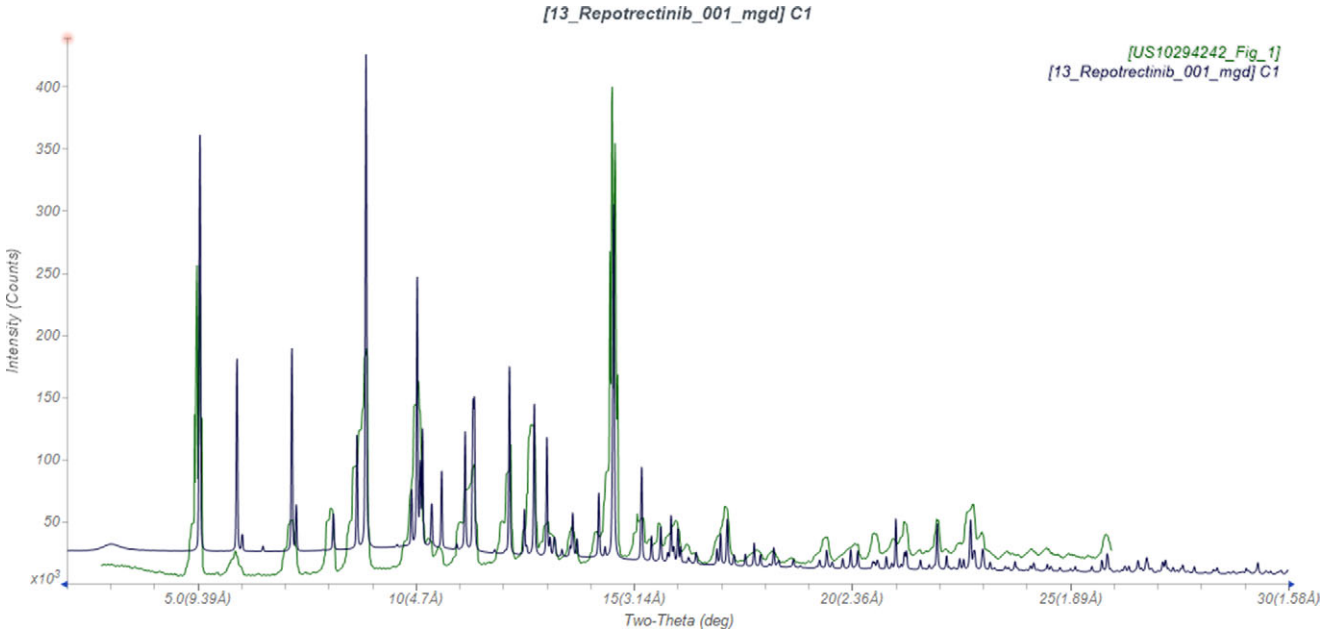

Figure 3. Comparison of the synchrotron pattern from this study of repotrectinib (black) to the laboratory pattern reported by Cui and Rogers (2019) (green). The literature pattern (measured using Cu K_α radiation) was digitized using UN-SCAN-IT (Silk Scientific, 2013) and converted to the synchrotron wavelength of 0.819563(2) Å using JADE Pro (MDI, 2024). Image generated using JADE Pro (MDI, 2024).

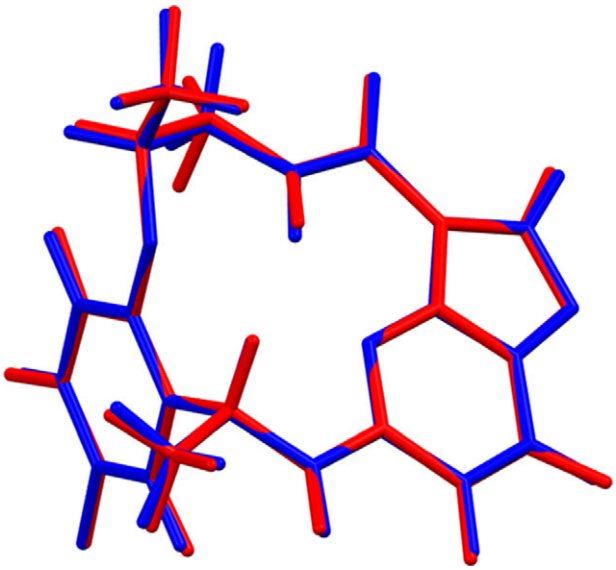

Figure 4. Comparison of the Rietveld-refined (red) and VASP-optimized (blue) structures of the repotrectinib molecule. The root-mean-square Cartesian displacement is 0.051 Å. Image generated using Mercury (Macrae et al., 2020).

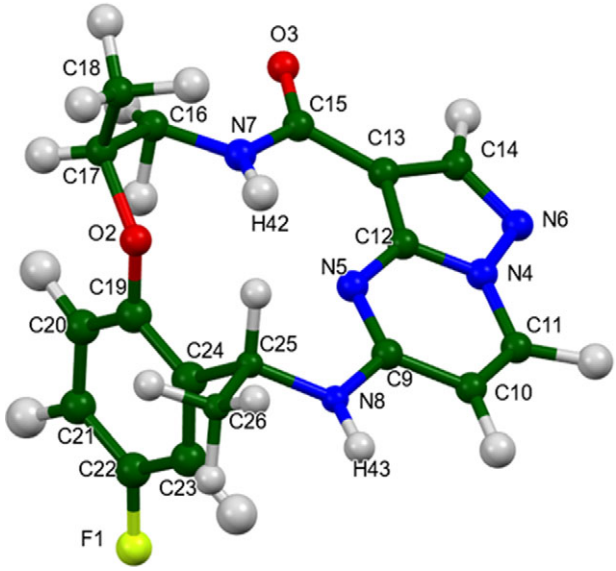

Figure 5. The asymmetric unit of repotrectinib, with the atom numbering. The atoms are represented by 50% probability spheroids. Image generated using Mercury (Macrae et al., 2020).

Streek and Neumann, 2014). The asymmetric unit is illustrated in Figure 5. The remaining discussion will emphasize the VASP-optimized structure.

Almost all of the bond distances, bond angles, and torsion angles fall within the normal ranges indicated by a Mercury Mogul Geometry check (Macrae et al., 2020). The O2–C17–C16 angle of 112.2° (average = 106.1(11)°, *Z*-score = 5.4) is flagged as unusual. There is only a small population of similar angles, and the standard uncertainty on the average is smaller than usual (inflating the *Z*-score). Torsion angles involving rotation about the O2–C17 bond lie on the tails of broad distributions. Torsion angles about C16–C17 lie on the tail of a narrow distribution or in a minor *gauche* population of mainly *trans* torsion angles. The conformation of the ether portion of the macrocycle is slightly unusual.

Quantum chemical geometry optimization of an isolated repotrectinib molecule (DFT/B3LYP/6-31G*/water) using Spartan '24 (Wavefunction, 2023) indicated that the observed molecule is 3.2 kcal/mol higher in energy than a local minimum, which has a very similar geometry (rms displacement = 0.203 Å). The global minimum-energy conformation (MMFF force field) is only 0.7 kcal/mol lower in energy and has a different orientation of the methyl group C15, along with other smaller local changes. The repotrectinib molecule is apparently flexible, and

https://doi.org/10.1017/S0885715625100882 Published online by Cambridge University Press

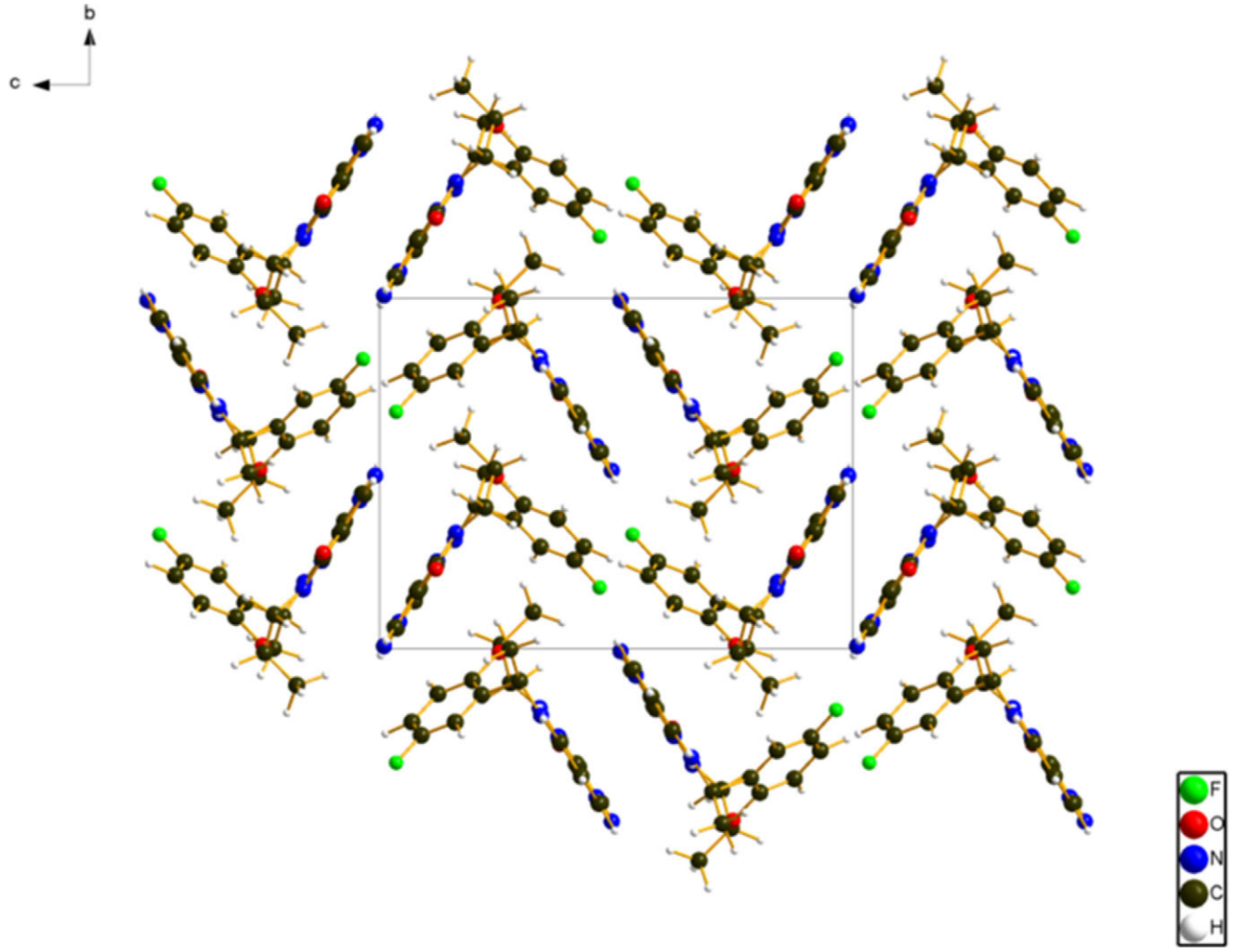

Figure 6. The crystal structure of repotrectinib, viewed down the *a*-axis. Image generated using Diamond (Crystal Impact, 2023).

intermolecular interactions have an effect on the solid-state conformation.

The crystal structure (Figure 6) consists of stacks of V-shaped molecules along the *b*-axis. The mean plane of the phenyl ring is approximately (−5, 12, 11), and the mean plane of the pyrazolo[1,5-*a*]pyrimidine ring system is approximately (0, −1, 2). The Mercury Aromatics Analyser indicates one moderate interaction between the phenyl rings, with a distance of 6.69 Å, as well as several weak interactions with distances of >7.0 Å. The shortest distance between the centroids of the pyrazolo[1,5-*a*]pyrimidine ring systems is 5.81 Å.

Analysis of the contributions to the total crystal energy of the structure using the Forcite module of Materials Studio (Dassault Systèmes, 2023) indicates that the intramolecular energy is dominated by angle distortion terms. The intermolecular energy is dominated by electrostatic attractions, which in this force-field-based analysis also include hydrogen bonds. The hydrogen bonds are better discussed using the results of the density functional theory (DFT) calculation.

There are several hydrogen bonds in the structure (Table I). The amino group N8–H43 acts as a donor to the carbonyl group O3 to link the molecules into chains along the *a*-axis with a graph set *C1,1(8)* (Etter, 1990; Bernstein et al., 1995; Motherwell et al., 2000). The amino group N7–H42 forms two intramolecular hydrogen bonds to N5 and O2. The energies of the N–H···O hydrogen bonds were calculated using the correlation of Wheatley and Kaduk (2019). Both intra- and intermolecular C–H···O hydrogen bonds, as well as a C–H···N hydrogen bond, also contribute to the lattice energy.

The volume enclosed by the Hirshfeld surface of repotrectinib (Figure 7; Hirshfeld, 1977; Spackman et al., 2021) is 414.04 Å^3, 98.39% of one-fourth of the unit cell volume. The packing density is thus typical. The only significant close contacts (red in Figure 7) involve the hydrogen bonds. The volume/non-hydrogen atom is smaller than usual at 16.8 Å^3.

The Bravais–Friedel–Donnay–Harker (Bravais, 1866; Friedel, 1907; Donnay and Harker, 1937) algorithm suggests that we might expect isotropic morphology for repotrectinib. A second-order spherical harmonic model was included in the refinement. The texture index was 1.015(0), indicating that the preferred orientation was insignificant in this rotated capillary specimen.

DEPOSITED DATA

The powder pattern of repotrectinib from this synchrotron dataset has been submitted to the International Centre for Diffraction Data (ICDD) for inclusion in the Powder Diffraction

https://doi.org/10.1017/S0885715625100882 Published online by Cambridge University Press

TABLE I. Hydrogen bonds (CRYSTAL23) in repotrectinib

H bond	D–H, Å	H···A, Å	D···A, Å	D–H···A, °	Mulliken overlap, *e*	*E*, kcal/mol
N8–H43···O3	1.029	2.008	2.988	158.3	0.053	5.3
N7–H42···N5	1.033	1.899[a]	2.793	142.9	0.063	
N7–H42···O2	1.033	2.327[a]	2.753	103.2	0.016	2.9
C10–H27···O3	1.089	2.363	3.245	136.9	0.024	
C17–H31···O3	1.102	2.415	3.300	136.2	0.015	
C25–H38···O2	1.100	2.296[a]	2.794	105.2	0.015	
C26–H39···N6	1.100	2.773	3.735	145.9	0.013	

[a]Intramolecular.

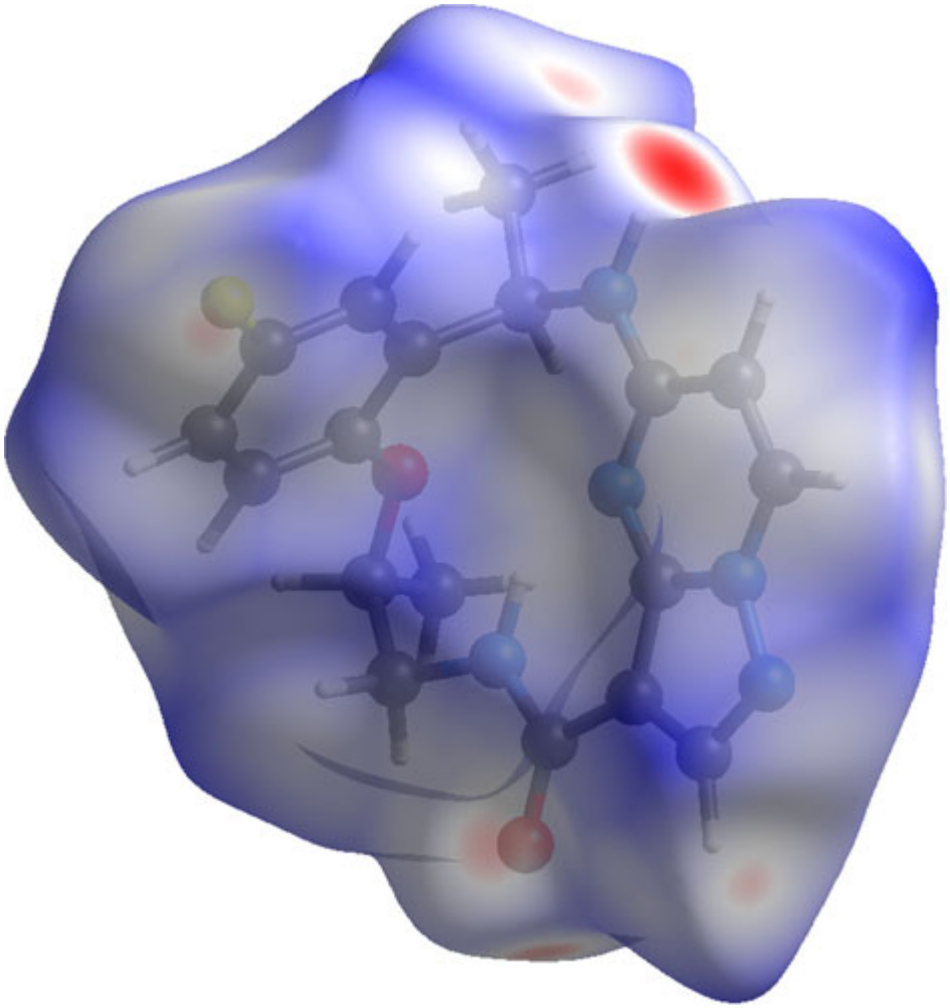

Figure 7. The Hirshfeld surface of repotrectinib. Intermolecular contacts longer than the sums of the van der Waals radii are colored blue/gray, and contacts shorter than the sums of the radii are colored red. Contacts equal to the sums of radii are white. Image generated using CrystalExplorer (Spackman et al., 2021).

File. The Crystallographic Information Framework (CIF) files containing the results of the Rietveld refinement (including the raw data) and the DFT geometry optimization were deposited with the ICDD. The data can be requested at pdj@icdd.com.

ACKNOWLEDGEMENTS

We thank Adam Leontowich for his assistance in the data collection. We also thank the ICDD team – Megan Rost, Steve Trimble, and Dave Bohnenberger – for their contribution to research, sample preparation, and in-house XRD data collection and verification.

FUNDING STATEMENT

Part or all of the research described in this paper was performed at the Canadian Light Source, a national research facility of the University of Saskatchewan, which is supported by the Canada Foundation for Innovation (CFI), the Natural Sciences and Engineering Research Council (NSERC), the Canadian Institute of Health Research (CIHR), the Government

https://doi.org/10.1017/S0885715625100882 Published online by Cambridge University Press

of Saskatchewan, and the University of Saskatchewan. This work was partially supported by the International Centre for Diffraction Data.

CONFLICTS OF INTEREST

The authors have no conflicts of interest to declare.

REFERENCES

Altomare, A., C. Cuocci, C. Giacovazzo, A. Moliterni, R. Rizzi, N. Corriero, and A. Falcicchio. 2013. "EXPO2013: A Kit of Tools for Phasing Crystal Structures from Powder Data." *Journal of Applied Crystallography* 46: 1231–35.

Bernstein, J., R. E. Davis, L. Shimoni, and N. L. Chang. 1995. "Patterns in Hydrogen Bonding: Functionality and Graph Set Analysis in Crystals." *Angewandte Chemie International Edition in English* 34: 1555–73.

Bravais, A. 1866. *Etudes Cristallographiques*. Gauthier Villars.

Bruno, I. J., J. C. Cole, M. Kessler, J. Luo, W. D. S. Motherwell, L. H. Purkis, B. R. Smith, et al. 2004. "Retrieval of Crystallographically Derived Molecular Geometry Information." *Journal of Chemical Information and Computer Sciences* 44: 2133–44.

Crystal Impact. 2023. *Diamond V. 5.0.0*. Crystal Impact – Dr. H. Putz & Dr. K. Brandenburg.

Cui, J. J., and E. W. Rogers. 2019. "Diaryl Macrocycle Polymorph." U.S. Patent 10294242 B2.

Dassault, Systèmes. 2023. *BIOVIA Materials Studio 2024*. San Diego, CA, BIOVIA.

Donnay, J. D. H., and D. Harker. 1937. "A New Law of Crystal Morphology Extending the Law of Bravais." *American Mineralogist* 22: 446–67.

Erba, A., J. K. Desmarais, S. Casassa, B. Civalleri, L. Donà, I. J. Bush, B. Searle, et al. 2023. "CRYSTAL23: A Program for Computational Solid State Physics and Chemistry." *Journal of Chemical Theory and Computation* 19: 6891–932. https://doi.org/10.1021/acs.jctc.2c00958.

Etter, M. C. 1990. "Encoding and Decoding Hydrogen-Bond Patterns of Organic Compounds." *Accounts of Chemical Research* 23: 120–26.

Friedel, G. 1907. "Etudes sur la loi de Bravais." *Bulletin de la Société Française de Minéralogie* 30: 326–455.

Gatti, C., V. R. Saunders, and C. Roetti. 1994. "Crystal-Field Effects on the Topological Properties of the Electron-Density in Molecular Crystals – the Case of Urea." *Journal of Chemical Physics* 101: 10686–96.

Groom, C. R., I. J. Bruno, M. P. Lightfoot, and S. C. Ward. 2016. "The Cambridge Structural Database." *Acta Crystallographica Section B: Structural Science, Crystal Engineering and Materials* 72: 171–79.

Hirshfeld, F. L. 1977. "Bonded-Atom Fragments for Describing Molecular Charge Densities." *Theoretica Chemica Acta* 44: 129–38.

Kabekkodu, S., A. Dosen, and T. N. Blanton. 2024. "PDF-5+: A Comprehensive Powder Diffraction File™ for Materials Characterization." *Powder Diffraction* 39: 47–59.

Kaduk, J. A., C. E. Crowder, K. Zhong, T. G. Fawcett, and M. R. Suchomel. 2014. "Crystal Structure of Atomoxetine Hydrochloride (Strattera), $C_{17}H_{22}NOCl$." *Powder Diffraction* 29: 269–73.

Kim S., J. Chen, T. Cheng, A. Gindulyte, J. He, S. He, Q. Li, et al. 2023. "PubChem 2023 Update." *Nucleic Acids Research* 51 (D1): D1373–80. https://doi.org/10.1093/nar/gkac956.

Kresse, G., and J. Furthmüller. 1996. "Efficiency of Ab-Initio Total Energy Calculations for Metals and Semiconductors Using a Plane-Wave Basis Set." *Computational Materials Science* 6: 15–50.

Leontowich, A. F. G., A. Gomez, B. Diaz Moreno, D. Muir, D. Spasyuk, G. King, J. W. Reid, C.-Y. Kim, and S. Kycia. 2021. "The Lower Energy Diffraction and Scattering Side-Bounce Beamline for Materials Science at the Canadian Light Source." *Journal of Synchrotron Radiation* 28: 1–9. https://doi.org/10.1107/S1600577521002496.

Macrae, C. F., I. Sovago, S. J. Cottrell, P. T. A. Galek, P. McCabe, E. Pidcock, M. Platings, et al. 2020. "*Mercury 4.0*: From Visualization to Design and Prediction." *Journal of Applied Crystallography* 53: 226–35.

Materials Design. 2024. *MedeA 3.7.2*. Materials Design, Inc.

MDI. 2024. *JADE Pro Version 9.0*. Materials Data.

Motherwell, W. D. S., G. P. Shields, and F. H. Allen. 2000. "Graph-Set and Packing Analysis of Hydrogen-Bonded Networks in Polyamide Structures in the Cambridge Structural Database." *Acta Crystallographica B* 56: 857–71.

Murray, B. W., E. Rogers, D. Zhai, W. Dong, X. Chen, P. A. Sprengeler, X. Zhang, et al. 2021. Molecular Characteristics of Repotrectinib That Enable Potent Inhibition of TRK Fusion Proteins and Resistant Mutations. *Molecular Cancer Therapeutics* 20: 2446–56.

Peintinger, M. F., D. Vilela Oliveira, and T. Bredow. 2013. "Consistent Gaussian Basis Sets of Triple-Zeta Valence with Polarization quality for Solid-State Calculations." *Journal of Computational Chemistry* 34: 451–59.

Silk Scientific. 2013. *UN-SCAN-IT 7.0*. Silk Scientific Corporation.

Spackman, P. R., M. J. Turner, J. J. McKinnon, S. K. Wolff, D. J. Grimwood, D. Jayatilaka, and M. A. Spackman. 2021. "CrystalExplorer: A Program for Hirshfeld Surface Analysis, Visualization and Quantitative Analysis of Molecular Crystals." *Journal of Applied Crystallography* 54: 1006–11. https://doi.org/10.1107/S1600576721002910; https://crystalexplorer.net.

Stephens, P. W. 1999. "Phenomenological Model of Anisotropic Peak Broadening in Powder Diffraction." *Journal of Applied Crystallography* 32: 281–89.

Sykes, R. A., P. McCabe, F. H. Allen, G. M. Battle, I. J. Bruno, and P. A. Wood. 2011. "New Software for Statistical Analysis of Cambridge Structural Database Data." *Journal of Applied Crystallography* 44: 882–86.

Toby, B. H., and R. B. Von Dreele. 2013. "GSAS II: The Genesis of a Modern Open Source All Purpose Crystallography Software Package." *Journal of Applied Crystallography* 46: 544–49.

van de Streek, J., and M. A. Neumann. 2014. "Validation of Molecular Crystal Structures from Powder Diffraction Data with Dispersion-Corrected Density Functional Theory (DFT-D)." *Acta Crystallographica Section B: Structural Science, Crystal Engineering and Materials* 70: 1020–32.

Wavefunction, Inc. 2023. *Spartan '24. V. 1.0.0. Placeholder Text*Placeholder TextWavefunction, Inc.

Wheatley, A. M., and J. A. Kaduk. 2019. "Crystal Structures of Ammonium Citrates." *Powder Diffraction* 34: 35–43.